

# Structural properties of silicon dioxide thin films densified by medium-energy particles

Alexis Lefèvre,<sup>a</sup> Laurent J. Lewis,<sup>a\*</sup> Ludvik Martinu,<sup>b</sup> Michael R. Wertheimer<sup>b</sup>

<sup>a</sup>*Département de Physique et Groupe de Recherche en Physique et Technologie des Couches Minces (GCM), Université de Montréal, Case Postale 6128, Succursale Centre-Ville, Montréal, Québec, Canada H3C 3J7*

<sup>b</sup>*Département de Génie Physique et de Génie des Matériaux et Groupe de Recherche en Physique et Technologie des Couches Minces (GCM), École Polytechnique de Montréal, Case Postale 6079, Succursale Centre-Ville, Montréal, Québec, Canada H3C 3A7*

(October 23, 2018)

Submitted to *Physical Review B*

Classical molecular-dynamics simulations have been carried out to investigate densification mechanisms in silicon dioxide thin films deposited on an amorphous silica surface, according to a simplified ion-beam assisted deposition (IBAD) scenario. We compare the structures resulting from the deposition of near-thermal (1 eV) SiO<sub>2</sub> particles to those obtained with increasing fraction of 30 eV SiO<sub>2</sub> particles. Our results show that there is an energy interval — between 12 and 15 eV per condensing SiO<sub>2</sub> unit on average — for which the growth leads to a dense, low-stress amorphous structure, in satisfactory agreement with the results of low-energy ion-beam experiments. We also find that the crossover between low- and high-density films is associated with a tensile to compressive stress transition, and a simultaneous healing of structural defects of the *a*-SiO<sub>2</sub> network, namely three- and four-fold rings. It is observed, finally, that densification proceeds through significant changes at intermediate length scales (4–10 Å), leaving essentially unchanged the “building blocks” of the network, viz. the Si(O<sub>1/2</sub>)<sub>4</sub> tetrahedra. This latter result is in qualitative agreement with the mechanism proposed to explain the irreversible densification of amorphous silica recovered from high pressures (~ 15–20 GPa).

PACS numbers: 61.43.Bn, 68.55.Ac, 77.55.+f, 81.15.Aa

## I. INTRODUCTION

In response to the rapidly increasing demand for highly-specialized applications in optical filtering devices, integrated electronics and photonics technology, considerable efforts have been devoted in the past few decades to the development of methods for growing thin silicon dioxide (SiO<sub>2</sub>) coatings having low stress and low defect concentrations, and exhibiting bulk-like optical properties. To this end, methods commonly referred to as ion-assisted deposition (IAD), in which growth is accompanied by a flux of energetic particles, are of particular interest:<sup>1–4</sup> indeed, bombardment with low to medium-energy neutral or ionic particles — in the range 10–200 eV — is found to have beneficial effects on a number of physical properties of the deposited material. Besides fulfilling the above requirements, it also leads to reduced moisture absorption, higher density, lower chemical etch rate, better adhesion to the substrate, and therefore better overall long-term behavior.<sup>5–7</sup> In addition, IAD methods allow processing at lower substrate temperatures, making them especially adapted to growth on polymers or graded-index coatings.<sup>1</sup> While there evidently exists a threshold energy below which benefits are insignificant, too high an energy can have undesirable consequences, such as preferential sputtering or impurity

incorporation.<sup>8</sup>

In ion-beam assisted deposition (IBAD) — a special case of IAD — an external source provides a well collimated flux of ions with a narrow kinetic energy distribution. It has proven useful to discuss the dependance of structural changes of IBAD films upon bombardment in terms of three parameters: the mean kinetic energy of the ions,  $E_i$ , the ratio of ion-to-condensing particle fluxes at the surface,  $\phi_i/\phi_n$  (where  $\phi_n$  is measured from the growth rate), and the energy delivered by each particle that condenses,  $E_p = E_i\phi_i/\phi_n$ .<sup>3,5,7</sup> It has been observed that there exist “critical” values of these parameters below which the films are porous and above which they are densely packed.<sup>3</sup> In the latter case, films are in general found to exhibit better physical properties, closer to their bulk, relaxed counterparts. For SiO<sub>2</sub>,  $E_p$ , determined from optical index, step coverage or optical transmittance measurements, is in the range 10–100 eV, depending on the particular set of parameters used in the growth process.<sup>3,5,7,9</sup>

Clearly, bombardment profoundly affects the microstructure of the deposited material. For amorphous solids — which is the case of SiO<sub>2</sub> films — static disorder hampers the measurement of detailed information beyond the second-neighbor shell. As a consequence, experimental results must be considered in the light of

structural models. In this way, proper conclusions on the atomic mechanisms that mediate bombardment-induced densification can be drawn. Thus, for instance, models help understanding how changes in the medium-range structure of amorphous silica ( $a\text{-SiO}_2$ ) influence the Si–O–Si bond-angle,<sup>10</sup> which in turn is related to such properties as the density, the optical index or the amount of built-in stress.<sup>1,5,7,11</sup>

It is useful to discuss the structure of  $a\text{-SiO}_2$  in terms of short-range order (SRO) and medium-range order (MRO) correlations,<sup>12</sup> at length scales  $\leq 4$  Å and in the range 4–10 Å, respectively. SRO is well defined in terms of such quantities as bond lengths and coordination numbers. It is mainly associated to the structural “building block” of the network, the  $\text{Si}(\text{O}_{1/2})_4$  tetrahedron. Both numerical simulations<sup>13–15</sup> and experiment<sup>16–18</sup> have shown the SRO correlations in permanently-densified (20%)  $a\text{-SiO}_2$  recovered from high pressures ( $\sim 15\text{-}20$  GPa) to be essentially the same as in the “normal” material.

In contrast, MRO correlations, which are at the origin of the so-called “first sharp diffraction peak” (FSDP), undergo important modifications upon compression:<sup>18–20</sup> the height of the FSDP decreases and its position increases with density. Molecular-dynamics<sup>13</sup> and Monte-Carlo<sup>15</sup> simulations have attributed this effect to modifications in the topology of the network; in particular, the intensity of the FSDP is reported to be roughly proportional to the number of six-membered rings. (A  $n$ -membered ring is defined as a closed loop of  $n$  Si–O bonds). Further, the x-ray diffraction spectra of porous silica thin films deposited at low substrate temperatures, using either electron-beam evaporation<sup>21</sup> or low-pressure chemical vapor deposition (LPCVD),<sup>22</sup> exhibit a strong low-angle scattering intensity and a FSDP height smaller than that of bulk  $a\text{-SiO}_2$ . The latter effect, which diminishes upon annealing, has been attributed to differences at the MRO level. However, to the best of our knowledge, no systematic studies of the changes in MRO with the kinetic energy of the ions or the ion-current density have so far been reported; this constitutes one objective of the present work.

Several computational methods have been employed to assess the role of ion beams during thin film growth.<sup>23</sup> Among them, molecular-dynamics (MD) simulations have provided useful insights into the understanding of ion-induced layer-by-layer growth,<sup>24</sup> surface mobility,<sup>25</sup> pore annihilation,<sup>26</sup> stress<sup>27</sup> and defect formation.<sup>28</sup> These studies have focused on the role of collision-induced events for obtaining crystalline material. Although the precise values of the parameters required for this purpose are material-dependent, a beam energy of the order of a few tens of eV — in agreement with experiment<sup>24,29</sup> — appears to be adequate, yielding ordered structures on the scale of many interatomic spacings. These simulations allow collision-induced events to be sorted out and relevant deposition parameters to be

identified, thus providing useful information for better control of the growth process.

The situation is more complicated for the case of amorphous materials growth, as spatial order is short-ranged. Only very few MD studies of the structural properties of amorphous thin film growth have thus far been reported; notable exceptions are Refs. 30,31 for silicon and Refs. 32,33 for diamond-like carbon films. In the latter case, bonding is found to be partly  $sp^2$  and partly  $sp^3$ , that is, between graphite and diamond. For the case of  $\text{SiO}_2$  — for which no such studies so far exist — considering the large number of polymorphs of the material,<sup>34</sup> as-deposited films are expected to show a large diversity of structures as a function of density.

In view of this, and given the technological importance of the material, we have carried out detailed MD simulations of the growth of silicon dioxide on  $a\text{-SiO}_2$  substrates. More precisely, growth is modelled within a simplified IBAD scenario: we examine, at the atomic level, how the structure of the films evolves as a function of  $R$ , the ratio of medium- (30 eV) to low-energy (1 eV)  $\text{SiO}_2$  particle fluxes impinging on the surface. The rationale for the model is given in Sec. II. For the sake of simplicity, the energetic ions are taken to be  $\text{SiO}_2$  “molecules”; although this is a very crude approximation to the real growth process, our model is expected to provide much-needed information into the fundamental aspects of bombardment-induced densification. We find, on average, that densification is related to changes in the ring structure, in a way which is similar to the case of pressure-induced densification of “normal” ( $2.2\text{ g/cm}^3$ ) silica glass. The intensity of the FSDP and the number of six-membered rings are here found to increase with density. We also find that the crossover from low- to high-density films is associated with a tensile-compressive stress transition, occurring for  $E_p$  of about 12–15 eV. It is observed, finally, that medium-energy bombardment promotes the annihilation of structural defects, namely three- and four-membered rings, which are at the origin of the  $D_2$  and  $D_1$  defect lines observed in the Raman spectrum of silica.<sup>35</sup>

## II. COMPUTATIONAL DETAILS

MD consists in integrating the classical equations of motion for a set of interacting particles. The interactions can be derived from first principles, or expressed in some effective, empirical form whose parameters are fitted to experimental data. The first-principles approach is very accurate, but does not allow large systems to be dealt with over “long” times cales. These limitations are not so much of a problem in the empirical approach, but accuracy and “transferability”, that is, the ability for a model potential to adequately describe a phase to which it was not fitted, is an issue. For the problem considered here, empirical potentials are unavoidable. The model devel-

oped by Nakano *et al.* has been successfully employed to describe the bulk and the surface of disordered phases of SiO<sub>2</sub>, *viz.* amorphous and porous silica,<sup>10,13,36–41</sup> which are evidently relevant to the present problem. In this model, silicon is assumed to be coordinated to four oxygen atoms, that is, the network is chemically ordered. The total potential energy of the system is the sum of two- and three-body contributions:

$$V = \sum_{i < j} V_{ij}^{(2)}(r) + \sum_{i, j < k} V_{ijk}^{(3)}(\vec{r}_{ij}, \vec{r}_{jk}), \quad (1)$$

where  $i$ ,  $j$ , and  $k$  run over all particles. The two-body term is written as

$$V_{ij}^{(2)}(r) = A_{ij} \left( \frac{\sigma_i + \sigma_j}{r} \right)^{n_{ij}} + \frac{Z_i Z_j}{r} e^{-\frac{r}{\lambda}} - \frac{\alpha_j Z_i^2 + \alpha_i Z_j^2}{2r^4} e^{-\frac{r}{\xi}}, \quad (2)$$

where the various terms represent the steric repulsion, the Coulomb interaction due to charge transfer, and a charge-dipole interaction due to atomic polarizability, respectively. The three-body term, which describes the covalent bonding, is expressed as

$$V_{ijk}^{(3)}(\vec{r}_{ij}, \vec{r}_{jk}) = B_i \exp\left(\frac{\mu}{r_{ij} - r_0} + \frac{\mu}{r_{jk} - r_0}\right) \times [\cos(\theta_{ijk}) - \cos(\theta_{ijk}^0)]^2 \times \Theta(r_0 - r_{jk})\Theta(r_0 - r_{ij}), \quad (3)$$

where  $\Theta$  is the Heaviside step function, and  $\theta_{ijk}^0$  is the equilibrium value of the  $(\vec{r}_{ji}, \vec{r}_{jk})$  bond angle. This term is calculated for nearest-neighbor Si–O–Si and O–Si–O triplets only. The model was fitted to various physical properties of bulk SiO<sub>2</sub>, such as cohesive energy, elastic constants and the phonon density of states; the values of the parameters can be found in Ref. 38.

As demonstrated by surface extended x-ray absorption fine structure and x-ray photoelectron spectroscopy measurements, the atomic structure of silica coatings strongly depends on the particular deposition process used:<sup>42,43</sup> both silicon and oxygen atoms can be found in different environments, allowing the presence of homoatomic bonds. This is particularly true when sub-oxides are formed. These effects are not considered in our model; thus, the role of structural defects — such as peroxide radicals and, more generally, homopolar bonds — on relaxation mechanisms are not taken into account. For the case of (nearly) stoichiometric situations, experimental data on SiO<sub>2</sub> produced by plasma enhanced chemical vapor deposition (PECVD),<sup>6</sup> RF sputtering,<sup>42</sup> secondary ion deposition,<sup>44</sup> and ion-beam deposition<sup>45</sup> indicate that the basic “building-block” of the network is the Si(O<sub>1/2</sub>)<sub>4</sub> tetrahedron. Thus, chemical ordering is expected to dominate in these cases, and the model potential of Nakano *et al.* is assumed to correctly describe atomic correlations.

In IBAD, silicon (di-)oxide is evaporated in a low-pressure oxygen atmosphere;<sup>2,9</sup> part of the condensing particles therefore have an energy smaller than 0.1 eV. Simultaneously, a beam of O<sup>+</sup>/O<sub>2</sub><sup>+</sup> ions with energy in the range 30–500 eV is directed onto the substrate, in order to promote surface relaxation as well as to hamper the formation of suboxides due to preferential sputtering of oxygen atoms. Although the experimental procedure is relatively simple, an atomistic description of it is a formidable task, as it requires an environment-dependent potential for oxygen ions, neutral gaseous particles, and for surface and bulk atoms. For simplicity, because large systems have to be dealt with, we describe the growth of silica in terms of a single type of condensing particle, namely SiO<sub>2</sub>, for *both* the deposited species and the incident energetic ions. Since the clusters are free to dissociate on the substrate (and actually do so), we expect this approximation to be of little consequence on the final structure of the deposited film. However, because oxygen atoms are preferentially sputtered as the deposited energy is raised (leading to a 10% deficit in the worst cases), SiO<sub>3</sub> clusters were introduced when necessary so as to maintain the stoichiometry at 2:1. Also, the energy transferred during a collision varies with the mass of the incoming particle, which, in turn, may influence the value for which dense films are obtained. Thus, care must be taken when comparing these results with experiment. We also neglect atomic ionisation and electronic loss during collisions, a reasonable approximation at low energies, especially for the case of insulators.<sup>32,46</sup> The present model is evidently crude, but we expect that the generic features of the structure will be relevant to real materials, even though the dynamics of the deposition process is not described precisely.

The substrate on which growth takes place consists of a  $27.59 \times 27.59 \times 10 \text{ \AA}^3$  amorphous slab containing 747 atoms, extracted from a bulk ( $27.59^3 \text{ \AA}^3$ ) sample prepared using the activation-relaxation technique (ART) of Barkema and Mousseau.<sup>47</sup> The substrate is first subjected to an extensive thermal annealing cycle in order to allow the surface to relax. A 3  $\text{\AA}$ -thick layer at the bottom is held fixed, in order to mimic a semi-infinite system, but also to prevent the substrate from moving because of momentum transfer from incoming atoms. The remaining 7  $\text{\AA}$  are coupled to a heat bath at room temperature, consistent with experiment.<sup>5,9</sup> Velocity renormalization was used to maintain the system at constant temperature.

SiO<sub>2</sub> particles of roughly thermal kinetic energy ( $E = 0.02 - 0.06 \text{ eV}$ ) were used in an attempt to first grow samples without bombardment. However, this led to unstable structures and to clusters of a dozen atoms desorbing from the growing film. Much better results were obtained with  $E = 1 \text{ eV}$ , an energy similar to that used by Hensel *et al.*<sup>31</sup> (2 eV) in their MD study of bombardment-induced epitaxial growth of elemental silicon. For the high-energy particles, we used 30 eV, as suggested by the experimental results of McNeil *et al.*<sup>9</sup> As noted pre-

viously, important process parameters are expressed in term of the ion-to-condensing particle fluxes ratio,  $\phi_i/\phi_n$ . However, this quantity is not known *a priori* ( $\phi_n$  is deduced from the measurement of the growth rate); thus, it is not an adequate parameter for monitoring the simulation procedure. Instead, we used, as other authors,<sup>31</sup> the ratio,  $R$ , of low-to-medium energy particle fluxes. Low- and high-energy particles were chosen at random according to the desired  $R$  value, and deposited at normal incidence onto the substrate. The equations of motion were integrated using the Verlet algorithm with an adaptive time step, so as to adjust to abrupt changes of the velocities during collisions.<sup>48</sup> The time interval between the deposition of two successive particles was chosen in such a way as to provide a reasonable compromise between computational effort and proper relaxation of the surface. In practice, we found it adequate to relax the system during 4 and 8 ps after depositing a low- and a high-energy particle, respectively, before a new particle was introduced.

As the film grows, “normal” thermal diffusion into the substrate is not sufficient to drain away the excess energy brought about by incoming particles. Therefore, the entire sample was submitted to a 1 ps thermalisation phase each time before introducing a new particle. Prior to this, the temperature was around 350 K and 320 K for 30 eV and 1 eV SiO<sub>2</sub> particles, respectively. Since the constants of diffusion are small at these temperatures, the equilibration procedure is expected not to interfere with the growth process in any significant manner.

Simulations were carried out for several values of the parameter  $R$ , namely 0, 0.08, 0.22, 0.38, 0.55, 0.73, 1.07, 1.53, 2 and 2.73. It can be determined *a posteriori* that these correspond to  $\phi_i/\phi_n$  values of 0, 0.07, 0.18, 0.32, 0.41, 0.49, 0.62, 0.75, 0.80 and 0.9, respectively. In each case, about 1300 atoms ( $\sim$ 430 clusters) were deposited. Following deposition, the samples were equilibrated during 20 ps at 300 K, after which a 40-ps microcanonical run was carried out in order to let the sample reach structural equilibrium. The corresponding “true” duration of simulated growth is about 3 ns. All calculations were performed using the program `groF`, a general-purpose MD code for bulk and surfaces developed by one of the authors (LJL).

### III. RESULTS AND DISCUSSION

#### A. Structure of samples grown *without* bombardment

In order to assess the role and importance of bombardment on the properties of the grown material, we first discuss the case  $R = 0$ , where all incoming particles have the same energy, *viz.* 1 eV. Figure 1 shows a snapshot of the system at the end of the run. The material is evidently highly disordered and porous. In Fig. 2, we plot, for this system, the corresponding integrated number of

atoms from the bottom of the simulation cell; we note that it increases approximately linearly with  $z$  in the region 13-53 Å. This portion will henceforth be referred to as the “bulk-like” part of the deposit, where structural analysis will be performed in order to limit artifacts due to the surface and the substrate. The same procedure is used for samples grown with bombardment, which leaves us with 20 to 40 Å of bulk material, about 1000 atoms in all cases.

The overall mass density in the bulk-like region of the slab,  $1.3\pm 0.1$  g/cm<sup>3</sup>, is about 40% less than the “normal” density of *a*-SiO<sub>2</sub> (2.2 g/cm<sup>3</sup>) and 12% less than the density of SiO<sub>2</sub> grown by electron-beam evaporation on a silicon substrate at room temperature.<sup>5</sup> The discrepancy between experimental and calculated densities is possibly due to the short duration of the simulation runs, which may not be long enough to allow complete relaxation, and thus full densification. (The computational effort required to achieve complete relaxation is formidable, and it constitutes one of the outstanding problems of disordered-system simulations). For this model of silica, it is worth noting that the density is close to the critical value of 1.4 g/cm<sup>3</sup>, below which pore percolation occurs and leads to fracture.<sup>40</sup> This was not observed here; however, as will be shown below, the film contains high tensile stress ( $\sim$  2 GPa). Thus, relaxation is expected to proceed by densification and/or fracture formation. This is consistent with the observation of reduced crack toughness and adhesion to the substrate for the case of coatings grown at low substrate temperature,  $T_S$ , with insufficient bombardment.<sup>4</sup>

We now discuss the structure and topology of the deposited material, in order to provide a reference for samples grown in the presence of bombardment (cf. Sec. III B). Figure 3 shows the total pair distribution function for the bulk-like part of the sample, as well as for bulk silica; also shown are the partial distributions  $g_{\text{SiSi}}$ ,  $g_{\text{SiO}}$  and  $g_{\text{OO}}$ . Here again, the amorphous character of the material is clearly evident: order beyond the nearest-neighbour shell rapidly fades out. The nearest-neighbor Si–O, Si–Si and O–O distances are listed in Table I, along with those of bulk *a*-SiO<sub>2</sub>,<sup>49</sup> as well as other material produced by secondary ion deposition (SID) at room temperature<sup>44</sup> and LPCVD at  $T_S = 430^\circ\text{C}$ ;<sup>22</sup> the calculated and experimental values are seen to be in satisfactory agreement. The partial pair correlations reveal a broadening of the first peak of the Si–Si distribution compared to the “normal” glass, presumably a consequence of the more disordered structure of the deposited film. Also, small pre-peaks to the left of the nearest-neighbour peak are seen to develop in the Si–Si and O–O correlation functions, at 2.45 and 2.32 Å respectively. As will be demonstrated below, these are due to the presence of two- and three-membered rings, leading to Si–O–Si and O–Si–O bond angles of 90 and 130 degrees, respectively.

In spite of the disordered nature of the network, the structural building block remains, to a good approximation, the Si(O<sub>1/2</sub>)<sub>4</sub> tetrahedron, even though it might

be slightly distorted. Indeed, the coordination of silicon atoms, calculated from the area under the first peak of  $g_{\text{SiO}}$ , is about 3.9. Further, as displayed in Fig. 4(a), the O–Si–O bond angle distribution has a major peak centred at  $109.7^\circ$ , the usual tetrahedral bond angle.

The topology of the network can be described more precisely in terms of rings of nearest-neighbor bonds, where an  $n$ -membered ring is defined as the shortest closed path of  $n$  Si–O bonds originating on a given silicon atom.<sup>13</sup> In normal silica glass, the statistics are dominated by five-, six-, and seven-fold rings.<sup>39</sup> Smaller rings are unlikely to occur because they are too expensive in terms of elastic bond-bending energy. The existence of “odd-numbered” rings results in a broad distribution of Si–O–Si bond angles. In the normal material, this distribution is centered around  $143^\circ$  and has a width of about  $25^\circ$ ,<sup>50</sup> as can be seen in Fig. 4(b). In contrast, the mean Si–O–Si bond angle for evaporated  $\text{SiO}_2$  is known from infrared spectroscopy measurements to be  $7\text{--}10^\circ$  smaller than in  $\alpha\text{-SiO}_2$ .<sup>5</sup> This is attributed to the presence of three- and four-membered rings, manifested by the presence of two sharp peaks at  $606$  and  $495\text{ cm}^{-1}$  in the Raman spectrum of chemical vapor deposited (CVD) films, produced at low substrate temperature.<sup>35</sup>

Such small rings are a common feature of disordered  $\text{SiO}_2$  networks, and they are a consequence of rapid quenching rates;<sup>35,56</sup> thus, they are also expected to be present in  $\text{SiO}_2$  produced using evaporation methods. In the present model, the fraction of three- and four-membered rings is about 0.1 and 0.15 per deposited silicon atom, respectively, roughly ten and two times that of normal  $\alpha\text{-SiO}_2$ .<sup>10</sup> The mean value of the Si–O–Si bond angle is  $139^\circ$ . These results are consistent with the above-mentioned experimental results for evaporated films. In addition, two-membered rings (edge-sharing tetrahedra) are present here, but absent in the normal material. As can be seen in Fig. 4(b), the presence of such highly-strained rings gives rise to a sharp peak at low angles,  $\sim 92^\circ$ , in the Si–O–Si bond angle distribution, while the distributions at high angles agree within statistical accuracy. The  $92^\circ$  peak is directly related to two-membered rings, as can be appreciated from Fig. 4(c), while three-membered rings give rise to a shoulder at about  $130^\circ$  in the bond-angle distribution.

## B. Structure of samples grown *with* bombardment

We now examine the structure of samples produced in the presence of bombardment. It is expected that the energy provided by energetic particles will have an “annealing” effect, thereby reducing the proportion of high-energy structures — mostly two- and three-fold rings.

Simulations were carried out for several values of the  $R$  parameter. As an example, we show in Fig. 5 the final configuration for  $R = 0.73$ . Comparing this with Fig. 1, the main role of bombardment — densification — is

clearly evident: the mass density of this new sample is  $\rho = 2.16 \pm 0.1\text{ g/cm}^3$ , much higher than the value of  $1.3\text{ g/cm}^3$  for the sample grown without bombardment, and close to  $2.2\text{ g/cm}^3$  for normal  $\alpha\text{-SiO}_2$ . (The density of  $\alpha$ -quartz is  $2.65\text{ g/cm}^3$ ). In Fig. 6(a), we plot  $\rho$  as a function of  $R$ ; it is seen to increase rapidly, reaching a plateau at about  $2.3\text{ g/cm}^3$  for  $R \geq 0.6 \equiv R_c$ . This “critical”  $R$  value roughly marks the crossover from a state of tensile stress (at small values of  $R$ ) to a state of compressive stress, as can be seen in Fig. 6(b) where the pressure is plotted vs  $R$ . Near  $R_c$ , the ratio of ion-to-condensing particle fluxes  $\phi_i/\phi_n \approx 0.4\text{--}0.5$ ; this yields a critical energy,  $E_c$ , for obtaining high-density, low-stress films,  $E_c = E_i\phi_i/\phi_n$ , on the order of  $12\text{--}15\text{ eV}$  per condensing  $\text{SiO}_2$  unit.

The calculated value of  $E_c$  is in reasonable agreement with experiment, considering the relatively crude nature of our model and the evident difficulty in measuring this quantity in a reliable manner. Indeed, values have been reported between  $10$  and  $100\text{ eV}$ .<sup>3,4</sup> Souche *et al.*,<sup>7</sup> for instance, gave  $35\text{ eV}$ , based on optical index measurements on  $\text{SiO}_2$  prepared by oxygen IBAD at  $T_S = 250^\circ\text{C}$ , for a beam energy  $E_i = 150\text{ eV}$ . McNeil *et al.*,<sup>9</sup> using a similar deposition process but lower  $E_i$ ,  $30\text{ eV}$ , found the optical transmittance to deteriorate with high ion current density, indicating that  $E_c$  is *smaller* than  $30\text{ eV}$ ; an estimate in the range  $10\text{--}20\text{ eV}$  has been given.<sup>52</sup> Finally, Al-Bayati *et al.*,<sup>45</sup> using  $10\text{ eV Si}^+/\text{O}^+$  ion beams to grow  $\text{SiO}_2$  on a silicon substrate at  $350^\circ\text{C}$ , found the interface to be smooth and free of strain, and the film to be of excellent quality, with no evidence of suboxides; thus,  $10\text{ eV}$  would appear to be an upper bound to  $E_c$ .

The structural changes which take place upon densification can be investigated in terms of short- and medium-range order modifications. At short range, Si–O and O–O nearest-neighbour distances are found to depend very little on  $R$ , and they are close to the values observed for the sample grown without bombardment (cf. Section III A). We note, however, a slight ( $\sim 2\%$ ) increase of the Si–Si distance, consistent with an increase of the Si–O–Si mean bond angle from  $139^\circ$  for  $R = 0$  to  $143^\circ$  for  $R = 2.73$ . The Si coordination, between  $3.90$  and  $3.96$ , shows no systematic variation with rising density.

However, the picture is quite different at intermediate length scales. In Fig. 7 we plot, for both  $R = 0$  and  $R = 2.73$ , the total pair distribution function,  $g(r)$ , and the running coordination number,  $N(r)$ ; the latter, essentially the integral of the former, gives the mean number of atoms within a sphere of radius  $r$  centered on an average atom, irrespective of the atomic species. It is clear that the  $N(r)$  curves for the two samples are very similar for  $r \leq 3\text{ \AA}$ , confirming the role of the  $\text{Si}(\text{O}_{1/2})_4$  tetrahedron as the structural building block (no homoatomic bonds are allowed in this model). Above this value, however, strong differences develop. Densification, therefore, involves structural modifications at or beyond second nearest-neighbors.

Amorphous silica is known to possess significant or-

der at medium range, manifested in the so-called “first sharp diffraction peak” (FSDP) at  $1.55 \text{ \AA}^{-1}$ , and observed in neutron and x-ray diffraction experiments.<sup>53</sup> Although the precise origin of this peak, in terms of stable entities, is still the matter of debate,<sup>53–55</sup> MD simulations by Nakano *et al.* have shown that its position and shape arise from correlations between atoms at distances as large as  $12 \text{ \AA}$ .<sup>39</sup> The FSDP can therefore be viewed as a signature of the presence of MRO in  $\alpha$ -SiO<sub>2</sub>. In order to assess this picture within the present approach, that is, to quantify possible modifications in MRO upon densification, we calculated the static structure factor,  $S(q)$ , which is also accessible experimentally. This is shown in Fig. 8 for the samples with  $R = 0$  and  $R = 2.73$ , as well as for  $\alpha$ -SiO<sub>2</sub> prepared using the ART method;<sup>47</sup> the curves were smoothed using Gaussian functions of width  $0.1 \text{ \AA}^{-1}$  so as to mimic thermal as well as experimental broadening. There is evidently very little difference from one sample to another for  $q$ -values larger than  $4 \text{ \AA}^{-1}$ , consistent with the existence of a structural unit common to all three networks. In contrast, the low- $q$  portion of the spectra exhibit significant differences. In particular, for  $q \lesssim 1 \text{ \AA}^{-1}$ , the intensity varies strongly with  $R$ , in a manner which is inversely related to the density.

While the finite size of the system, plus periodic boundary conditions, artificially contribute to the intensity at such low- $q$  values, they cannot be solely responsible for the observed variations. Since all three samples are treated in the same manner and are similar in size, these variations must be related to the presence of pores in the low-density samples, an effect which can be understood in term of a Babinet argument — the scattering by a pore is similar to that from a cluster having comparable dimensions.

Changes in the MRO upon densification are also apparent in the FSDP, which the present model places at about  $1.60 \text{ \AA}^{-1}$ , in satisfactory agreement with the experimental value,  $1.55 \text{ \AA}^{-1}$ . For  $R = 0$ , that is, highly porous material, the FSDP shows up as a mere shoulder, whose intensity is 23% smaller than that of  $\alpha$ -SiO<sub>2</sub>. For  $R = 2.73$ , a well-defined peak is observed, which is only 7% smaller than that of the normal material. The complete picture is provided in Fig. 9, where we plot the intensity of the FSDP as a function of density. Although the statistics are not perfect, there is a clear tendency for the height of the FSDP to increase with increasing density. It is interesting to note that if the densification were the consequence of a homogenous elastic compression of the network, that is, without structural modifications, the mean atomic distances would decrease with increasing density, implying an overall shift of  $S(q)$  towards higher  $q$  values. Here, although the FSDP position is modified, no obvious trend is found.

The differences in heights of the FSDP among the various samples are consistent with the results of Himmel *et al.*,<sup>21</sup> who found a 28% smaller height in the x-ray static structure factor of electron-beam evaporated silica, compared with bulk fused silica. Our calculations

are also in qualitative agreement with MD simulations of pressure-induced densification of silica nanophases, where the height of the FSDP was found to be 15 % smaller compared to  $\alpha$ -SiO<sub>2</sub> in the density range  $1.67$  to  $2.03 \text{ g/cm}^3$ .<sup>36</sup>

The ring structure of the various models can tell us more about changes in MRO upon densification: because the size of rings is typically in the range  $4$ – $10 \text{ \AA}$ ,<sup>10</sup> modifications in the MRO are related to those in the arrangements of neighboring Si(O<sub>1/2</sub>)<sub>4</sub> tetrahedra. The occurrence of the various types of rings as a function of  $R$ , relative to  $R = 0$ , is shown in Fig. 10. In spite of statistical uncertainties, the following clear trends can be identified. (i) The number of two-, three- and four-membered rings decreases with rising  $R$ ; indeed, as noted in Sec. III A, these correspond to high-energy structures and therefore are expected to anneal out during low-energy bombardment. (ii) The number of five-, six-, and seven-membered rings increases with rising  $R$ ; these rings being close to the most probable size in  $\alpha$ -SiO<sub>2</sub>, they are thus strongly favored. (iii) The number of nine-membered rings decreases with density, indicating a reduction in the number of pores. In contrast, the relative occurrence of eight-membered rings exhibits no clear trend, most likely because they are relatively stable entities in dense, crystalline forms of silica, such as  $\alpha$ -quartz ( $2.65 \text{ g/cm}^3$ ) and coesite ( $2.92 \text{ g/cm}^3$ ).<sup>34</sup>

MD simulations on elemental silicon growth<sup>30,31</sup> have demonstrated, in agreement with experiments, that low-energy ion bombardment has an effect similar to annealing. For the case of SiO<sub>2</sub> prepared by IBAD, our results indicate that the elimination of two-, three- and four-fold rings may be achieved with the use of a second particle beam with kinetic energy in the range  $12$ – $15 \text{ eV}$ . The concentration of three- and four-fold rings was reported to decrease for CVD SiO<sub>2</sub> submitted to annealing;<sup>56</sup> however, to the best of our knowledge, no such investigation has been reported regarding their dependence upon IBAD ion-current density or ion kinetic energy. Such data would be of utmost interest.

The modifications in the ring statistics were pointed out in MD and Monte-Carlo simulations of pressure-induced densification of bulk silica.<sup>13,15</sup> It was found that most topological modifications are mediated by defect annihilation and bond switching. The former mechanism proceeds through the formation of bonds between non-bridging oxygen and three-fold coordinated silicon atoms, while the latter involves the diffusion of coordination defects (hopping of a dangling bond from one atom to a neighbor, accompanied by the formation of a new bond).<sup>15</sup> This has also been identified as an important relaxation mechanism in  $\alpha$ -SiO<sub>2</sub>, and it appears to be characteristic of chemically-ordered networks.<sup>47</sup> The latter point being an assumption of our model, it is expected that these mechanisms also play an important role during bombardment-induced densification. More precisely, since coordination numbers do not show systematic variations with increasing density, bond-switching is expected

to dominate over the annihilation of coordination defects.

In pressure-densified material, the evolution of the ring populations is quite different from the one we observe: the number of four-, eight-, and nine-fold rings increase, while those of five- and six-fold rings, as well as the intensity of the FSDP, decrease with increasing density (in the range 2.2–3.2 g/cm<sup>3</sup>). Taken together with the present results, this may indicate that in its most stable form, *a*-SiO<sub>2</sub> has maximum MRO at ambient temperature and pressure.

#### IV. CONCLUDING REMARKS

In this article, we have presented the results of extensive and detailed molecular-dynamics simulations of the growth of SiO<sub>2</sub> on a *a*-SiO<sub>2</sub> substrate, with a view of understanding the process of densification induced by low-energy particle bombardment. The physical picture which emerges from our observations is the following: the network undergoes significant density variations through structural changes at an intermediate length scale; more precisely, ring statistics are affected, while the structural unit of the network — the Si(O<sub>1/2</sub>)<sub>4</sub> tetrahedron — remains essentially unchanged. Upon bombardment, small rings, which are associated with defects in the network, rearrange to produce larger ones, thus reducing the energy cost associated with bond bending and increasing the mean Si–O–Si bond angle. Large rings, particularly nine-membered ones, “disintegrate” into five-, six-, and seven-membered rings, thus reducing the occupied volume and causing the density to increase. Simultaneously, this influences the intensity of the first sharp diffraction peak (FSDP), which is found to increase with rising density. By calculating the pressure inside the sample, we have found an “optimal” incident energy range for low-stress, high-density films of 12 to 15 eV per condensing SiO<sub>2</sub> particle.

The very brief (~4 ns) real-time equivalent duration of our simulations may not be sufficient to allow the samples to escape from local minima in the potential energy surface, leading to structures which are incompletely relaxed compared to the real material. Because relaxation processes, which are expected to increase MRO correlations, may occur within the time scale of an experiment, control over the film microstructure may be a difficult objective to attain when performing ion-assisted deposition experiments. In addition, most of MRO modifications arise from low-energy bombardment. For this reason, and as demonstrated by experimental results,<sup>9,45</sup> we emphasize that any deposition process where the average ion kinetic energy is greater than about ten eV should be avoided. Besides ion-beam experiments, it was recently demonstrated that magnetron sputtering processes could produce low-energy high ion flux (up to 30 ions per neutral condensing particle), allowing amorphous silicon films with a tunable amount of MRO to be grown.<sup>57</sup> We ex-

pect that such findings will stimulate further experiments on SiO<sub>2</sub> films, which will allow our results to be assessed. For example, a systematic study of the peaks associated with three- and four-membered rings in the Raman spectra of silica coatings, and the evolution of the FSDP, with the kinetic energy and flux of ions could help enhance our understanding of bombardment-induced densification.

*Acknowledgments* – A. L. is grateful to Gilles Denler for useful discussions. Normand Mousseau is acknowledged for providing the ART model. This work is supported by grants from the Natural Sciences and Engineering Research Council of Canada (NSERC) and by the “Fonds pour la formation de chercheurs et l’aide à la recherche” (FCAR) of the Province of Québec. We are indebted to the “Réseau québécois de calcul de haute performance” (RQCHP) for generous allocations of computer resources.

---

\* To whom correspondence should be addressed; electronic mail: Laurent.Lewis@UMontreal.CA

<sup>1</sup> L. Martinu and D. Poitras, *J. Vac. Sci. Technol. A* **18**, 2627 (2000).

<sup>2</sup> H. K. Pulker, *Surf. Coat. Technol.* **112**, 250 (1999).

<sup>3</sup> *Handbook of plasma processing technology*, edited by S. M. Rossnagel, J. J. Cuomo and W. D. Westwood, (Noyes Publications, Park Ridge, 1990).

<sup>4</sup> F. A. Smidt, *Int. Mat. Rev.* **35**, 61 (1990).

<sup>5</sup> A. Brunet-Bruneau, D. Souche, S. Fisson, V. Nguyen Van, G. Vuye, F. Abeles, and J. Rivory *J. Vac. Sci. Technol. A* **16**, 2281 (1998); A. Brunet-Bruneau, J. Rivory, B. Rafin, J. Y. Robic, and P. Chaton, *J. Appl. Phys.* **82**, 1330 (1997).

<sup>6</sup> M. V. Bazylenko, M. Gross, and D. Moss, *J. Appl. Phys.* **81**, 7497 (1997).

<sup>7</sup> D. Souche, A. Brunet-Bruneau, S. Fisson, V. Nguyen Van, G. Vuye, F. Abeles, and J. Rivory, *Thin Solid Films* **313-314**, 676 (1998).

<sup>8</sup> L. Martinu, J. E. Klemberg-Sapieha, O. M. Küttel, A. Raveh, and M. R. Wertheimer, *J. Vac. Sci. Technol. A* **12**, 1360 (1994).

<sup>9</sup> J. R. McNeil, A. C. Barron, S. R. Wilson, and W. C. Hermann, Jr., *Appl. Opt.* **23**, 552 (1984).

<sup>10</sup> J. Rino, I. Ebbsjö, R. Kalia, A. Nakano, and P. Vashishta, *Phys. Rev. B* **47**, 3053 (1993).

<sup>11</sup> G. Lucovsky, J. Manitini, J. K. Srivastava, and E. A. Irene, *J. Vac. Sci. Technol. B* **5**, 530 (1987).

<sup>12</sup> P. Vashishta, R. Kalia, J. Rino, and I. Ebbsjö, *Phys. Rev. B* **41**, 12197 (1990).

<sup>13</sup> J. Rino, G. Gutiérrez, I. Ebbsjö, R. Kalia, and P. Vashishta, in *Materials Theory, Simulations, and Parallel Algorithms*, edited by E. Kaxiras, J. Joannopoulos, P. Vashishta, and R. K. Kalia (Mat. Res. Soc. Symp. Proc. **408**, Philadelphia, PA, 1996), 333.

<sup>14</sup> J. S. Tse, D. D. Klug, and Y. Lepage, *Phys. Rev. B* **46**,

- 5933 (1992).
- <sup>15</sup> L. Stixrude and M. S. T. Bukowinski, *Phys. Rev. B* **44**, 2523 (1991).
- <sup>16</sup> R. A. B. Devine, R. Dupree, I. Farnan, and J. J. Capponi, *Phys. Rev. B* **35**, 2560 (1987).
- <sup>17</sup> R. A. B. Devine and J. Arndt, *Phys. Rev. B* **35**, 9376 (1987).
- <sup>18</sup> S. Susman, K. J. Volin, D. L. Price, M. Grimsditch, J. P. Rino, R. K. Kalia, P. Vashishta, G. Gwanmesia, Y. Wang, and R. C. Libermann, *Phys. Rev. B* **43**, 1194 (1991).
- <sup>19</sup> C. Z. Tan and J. Arndt, *J. Non-Cryst. Solids* **249**, 47-50 (1998).
- <sup>20</sup> S. Sugai and A. Onodera, *Phys. Rev. Lett.* **77**, 4210 (1996).
- <sup>21</sup> B. Himmel, T. Gerber, and H. G. Neumann, *Phys. Stat. Sol. A* **88**, K127 (1985).
- <sup>22</sup> J. Konnert, P. d'Antonio, M. Huffman, and A. Navrotsky, *J. Am. Ceram. Soc.* **70**, 192 (1987).
- <sup>23</sup> *Thin Films, Modeling of Film Deposition for Microelectronic Applications*, vol. **22**, edited by S. Rosnagel and A. Ulman, ( Academic Press, New-York, 1996).
- <sup>24</sup> J. Jacobsen, B. H. Cooper, and J. P. Sethna, *Phys. Rev. B* **58**, 15847 (1998).
- <sup>25</sup> T. Ohira, O. Ukai, T. Adachi, Y. Takeushi, and M. Murata, *Phys. Rev. B* **52**, 8283 (1995).
- <sup>26</sup> L. Dong, R. W. Smith, and D. J. Srolovitz, *J. Appl. Phys.* **80**, 5682 (1996).
- <sup>27</sup> C.-C. Fang, V. Prasad, R. V. Joshi, F. Jones, and J. J. Hsieh, in Ref. 23, 117.
- <sup>28</sup> J. Kitabatake and J. E. Greene, *J. Appl. Phys.* **73**, 3183 (1993).
- <sup>29</sup> G. K. Hubler, *Proceedings of the conference on Beam-Solids Interactions for Materials Synthesis and Characterization*, edited by D. C. Jacobson, D. E. Luzzi, T. F. Heinz, and M. Iwaki (*Mat. Res. Soc.* **354**, Pittsburg, 1995), 45.
- <sup>30</sup> B. Strickland and C. Roland, *Phys. Rev. B* **51**, 5061 (1995).
- <sup>31</sup> H. Hensel and H. M. Urbassek, *Phys. Rev. B* **58**, 2050 (1998).
- <sup>32</sup> H. P. Kaukonen and R. M. Nieminen, *Phys. Rev. Lett.* **68**, 620 (1992).
- <sup>33</sup> H. U. Jäger and K. Albe, *J. Appl. Phys.* **88**, 1129 (2000).
- <sup>34</sup> F. Liebau, in *The physics and technology of amorphous SiO<sub>2</sub>*, edited by R. A. B. Devine (Plenum, New-York, 1988), 15.
- <sup>35</sup> R. A. B. Devine and M. Marchand, *Appl. Phys. Lett.* **63**, 619 (1993).
- <sup>36</sup> T. Campbell, R. Kalia, A. Nakano, F. Shimojo, K. Tsuruta, P. Vashishta, and S. Ogata, *Phys. Rev. Lett.* **82**, 4018 (1999).
- <sup>37</sup> P. Vashishta, R. Kalia, A. Nakano, W. Li, and I. Ebbsjö, in *Amorphous Insulators and Semiconductors*, edited by M. F. Thorpe and M. I. Mitkova, (Kluwer, Dordrecht, 1997), 151.
- <sup>38</sup> A. Nakano, L. Bi, R. Kalia, and P. Vashishta, *Phys. Rev. B* **49**, 9441 (1994).
- <sup>39</sup> A. Nakano, R. Kalia, and P. Vashishta, *J. Non-Cryst. Solids* **171**, 157 (1994).
- <sup>40</sup> A. Nakano, R. Kalia, and P. Vashishta, *Phys. Rev. Lett.* **73**, 2336 (1994).
- <sup>41</sup> M. I. Trioni, A. Bongiorno, and L. Colombo, *J. Non-Cryst. Solids* **220**, 164 (1997).
- <sup>42</sup> A. J. Forty, M. Kerkar, J. Robison, S. M. El-Mashri, and E. N. Farrabaugh, *J. Phys.* **C8**(47), 857 (1986).
- <sup>43</sup> S. K. Ray, C. K. Maiti, S. K. Lahiri, and N. B. Chakrabarti, *J. Vac. Sci. Technol. B* **10**, 1139 (1992).
- <sup>44</sup> C. F. George and P. D'Antonio, *J. Non-Cryst. Solids* **34**, 323 (1979).
- <sup>45</sup> A. H. Al-Bayati, S. S. Todorov, K. J. Boyd, D. Marton, J. W. Rabalais and J. Kulik, *J. Vac. Sci. Technol. B* **13**, 1639 (1995).
- <sup>46</sup> M. Hedström and H. P. Cheng, *Phys. Rev. B* **59**, 10701 (1999).
- <sup>47</sup> N. Mousseau, *J. Chem. Phys.* **112**, 960 (2000).
- <sup>48</sup> R. Smith, M. Jakas, D. Ashworth, B. Oven, M. Bowyer, I. Chakarov, and R. Webb, in *Atomic and ion collisions in solids and at surfaces*, edited by R. Smith (Cambridge University Press, Cambridge, 1997), 247.
- <sup>49</sup> P. A. V. Johnson, A. C. Wright, and R. N. Sinclair, *J. Non-Cryst. Solids* **58**, 109 (1983).
- <sup>50</sup> S. L. Chan, L. F. Gladden, and S. R. Elliott, in Ref. 34, 83.
- <sup>51</sup> A. Pasquarello and R. Car, *Phys. Rev. Lett.* **80**, 5145 (1998).
- <sup>52</sup> J. M. E. Harper, J. J. Cuomo, R. J. Gambino, and H. R. Kaufman, *Nucl. Instrum. Meth. Phys. Res.* **B7/8**, 886 (1985).
- <sup>53</sup> S. C. Moss and D. L. Price, in *Physics of disordered materials*, edited by D. Adler, H. Fritzsche, and S. R. Ovshinsky (Plenum, New-York, 1985), 77.
- <sup>54</sup> S. R. Elliott, *J. Phys.: Cond. Mat.* **4**, 7661 (1992).
- <sup>55</sup> P. H. Gaskell and D. J. Wallis, *Phys. Rev. Lett.* **76**, 66 (1996).
- <sup>56</sup> P. McMillan, in Ref. 34, 63.
- <sup>57</sup> J.E. Gerbi, P.M. Voyles, M.M.J. Treacy, J.M. Gibson, and J.R. Abelson, unpublished

TABLE I. Nearest-neighbor distances and Si–O–Si mean bond angle, calculated for a sample grown without bombardment, along with those of SiO<sub>2</sub> produced by secondary ion deposition (SID), electron beam evaporation, low-pressure chemical vapor deposition (LPCVD), and bulk amorphous silica. Bond lengths are given in Å; in parentheses are the standard deviations.

	Si–Si	Si–O	O–O	Si–O–Si
This work	3.0 (0.17)	1.61 (0.05)	2.64 (0.1)	139°
SID a-SiO <sub>2</sub> <sup>44</sup>	3.06 (0.02)	1.61 (0.01)	2.64 (0.02)	144.6°
e-beam a-SiO <sub>2</sub> <sup>5</sup>				136°
LPCVD a-SiO <sub>2</sub> <sup>22</sup>	3.08 (0.13)	1.61 (0.06)	2.60 (0.1)	
a-SiO <sub>2</sub> <sup>49,50</sup>	3.08 (0.1)	1.61 (0.05)	2.63 (0.08)	143°



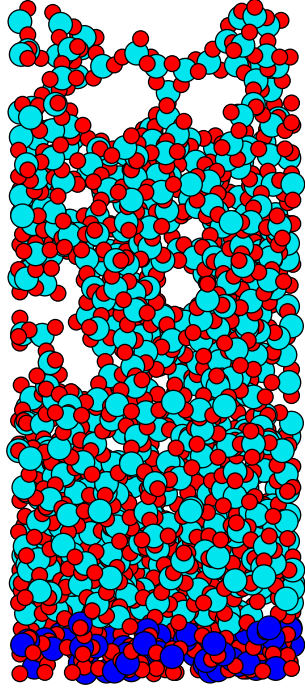


FIG. 1. Snapshot of the sample grown with 1 eV clusters. The total number of atoms is 2040. Silicon atoms are in light grey while oxygen atoms are dark grey. Darker atoms at the bottom of the cell indicate the fixed layers in the substrate region.

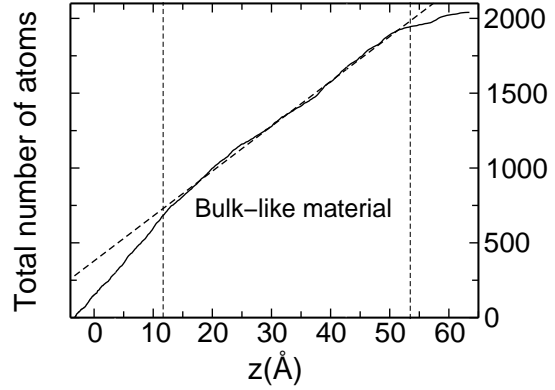


FIG. 2. Total (integrated) number of atoms as a function of the distance from the bottom of the cell for the sample grown without bombardment ( $R = 0$ ). The dashed curve is the best linear fit to the data in the bulk-like region of the sample (as indicated).

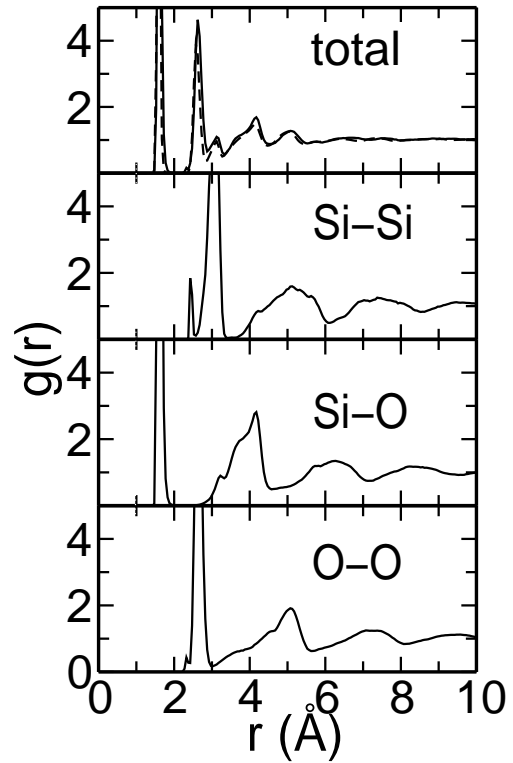


FIG. 3. Total and partial pair distribution functions calculated for a sample grown without bombardment ( $R = 0$ ). In the top panel, the dashed line shows the total pair distribution function for bulk amorphous silica prepared using ART.<sup>47</sup>

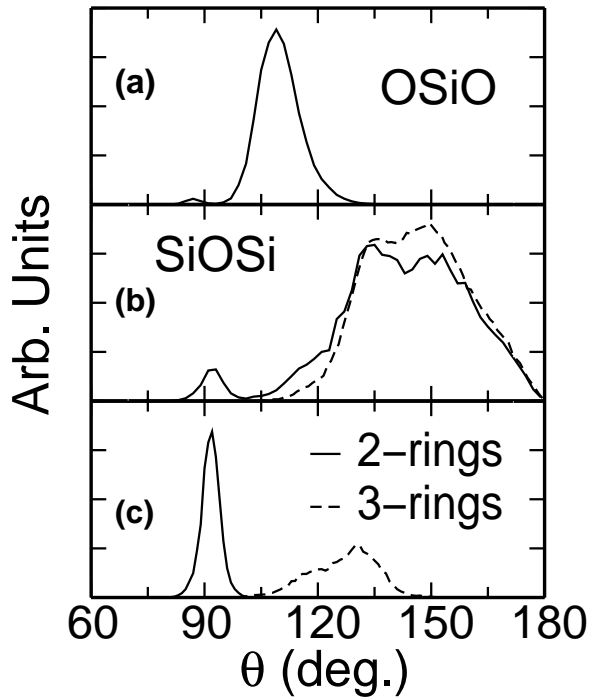


FIG. 4. Bond-angle distributions for a sample grown without bombardment: (a) O-Si-O; (b) Si-O-Si; also shown is the corresponding distribution for bulk-amorphous silica produced with ART (dashed line); (c) Si-O-Si for the special cases of two- and three-membered rings.

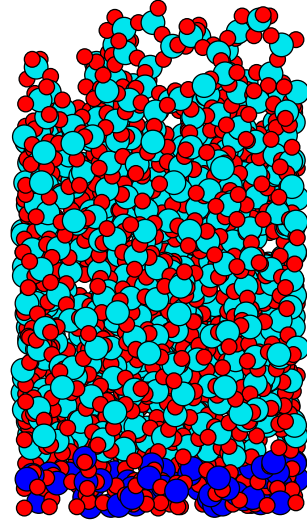


FIG. 5. Snapshot of the samples grown with  $R=0.73$ . The total number of atoms is 2040. The effect of bombardment is clearly visible when comparing to  $R=0$ .

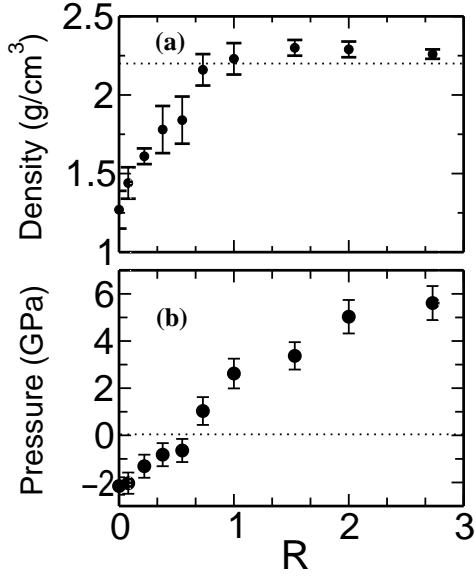


FIG. 6. (a) Density and (b) pressure versus  $R$  in the bulk part of the various samples; in (a), the dotted line indicates the density of bulk silica ( $2.2 \text{ g/cm}^3$ ); the error bars correspond to the calculated standard deviations.

FIG. 7. Total pair distribution function,  $g(r)$ , and running coordination number,  $N(r)$ , for the samples grown with  $R = 0$  and  $R = 2.73$ , as indicated. The inset is a magnification of  $N(r)$  in the region  $1.4\text{--}3.5 \text{ \AA}$ .

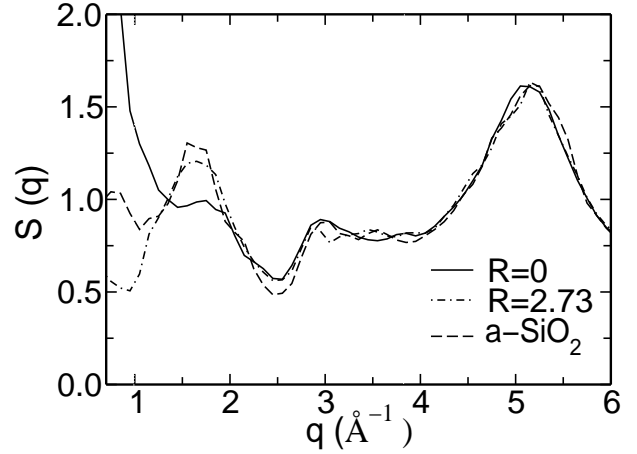


FIG. 8. Total static structure factor for the samples with  $R = 0$ ,  $R = 2.73$ , and for amorphous silica. Data are truncated at  $0.7 \text{ \AA}^{-1}$  due to the finite-size of the simulation cell.

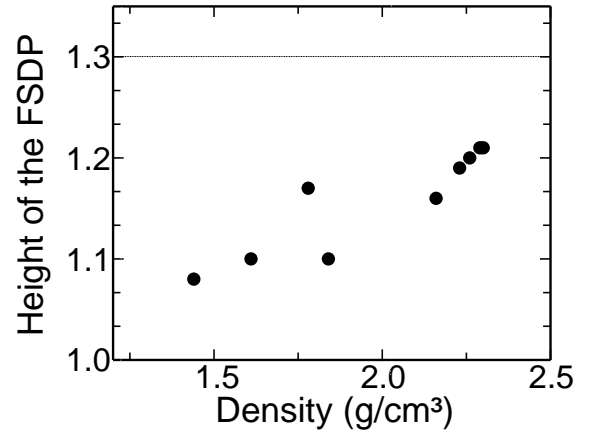
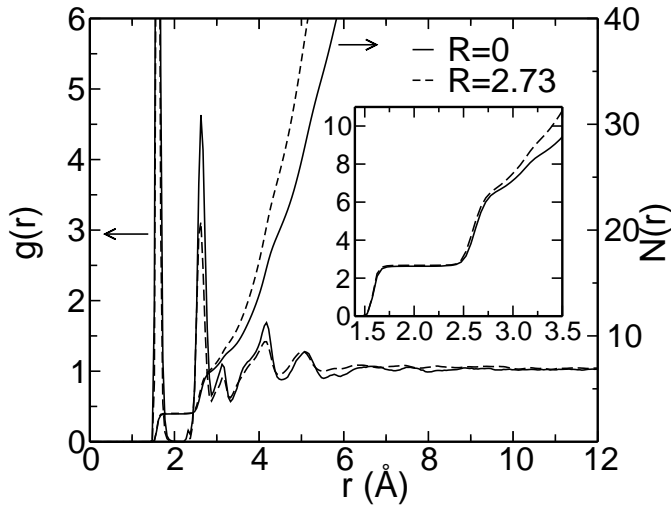


FIG. 9. Height of the first sharp diffraction peak as a function of the density of the samples. The dashed line is the corresponding value for  $a\text{-SiO}_2$  prepared using ART.<sup>47</sup>

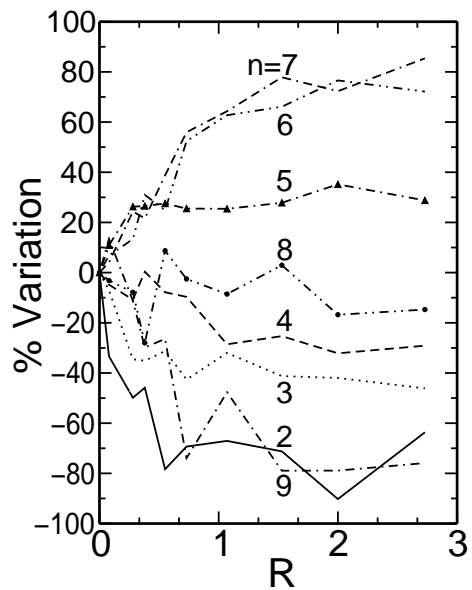


FIG. 10. Relative variation of the number of  $n$ -membered rings per silicon atom as a function of  $R$ .